Importance of tides and winds in influencing the nonstationary behaviour of coastal currents in offshore Singapore

Jun Yu Puah[1,2], Ivan D. Haigh[3], David Lallemant[1,2], Kyle Morgan[1,2], Dongju Peng[4], Masashi Watanabe[2], Adam D. Switzer[1,2]

[1]Asian School of the Environment, Nanyang Technological University, Singapore

[2]Earth Observatory of Singapore, Nanyang Technological University, Singapore

[3]School of Ocean and Earth Science, National Oceanography Centre Southampton, University of Southampton, Southampton, UK

[4]Department of Land Surveying and Geo-Informatics, The Hong Kong Polytechnic University, Hong Kong

Correspondence to: Jun Yu Puah (a210012@e.ntu.edu.sg)

Abstract. Coastal currents significantly impact port activities, coastal landform morphodynamics and ecosystem functioning. It is therefore necessary to understand the physical characteristics and natural variability of these currents within coastal settings. Traditional methods such as harmonic analysis assume stationarity of tide-driven currents and thus may not be applicable to systems modulated by variable nontidal inputs and processes. Here we deployed eight tilt current meters at shallow (< 5 m) coral reef environments in southern Singapore. Tilt current meters were positioned around the reefs at the main compass bearings to analyse the spatiotemporal variability of coastal currents in the frequency domain for one year (March 2018 to March 2019). Tidal motions were the primary mechanism of current flow on reefs and account for between 14–45 % of total variance across all sites, with diurnal currents having either similar or greater proportion of energy than semidiurnal currents. The relationship between currents and wind stress was then investigated across various frequencies. There is high correlation at low frequencies during the northeast monsoon, when the Madden-Julian oscillation (MJO) is more active and thus generates currents that propagate either in phase or ahead of the MJO. At diurnal frequencies, the interaction between P_1 and K_1 results in a semi-annual cycle where currents are stronger during the monsoon seasons. This interaction could help to explain the seasonal variation of correlation as well as the K_1 amplitude, the latter which could be further enhanced by the diurnal wind stress. The phase relationship between currents and wind stress is highly complex due to the variable bathymetry and could only be partially accounted for by the orientation of the coastlines relative to that of the wind. Given the importance of wind, we thus require longer time-series datasets to examine the role of atmospheric phenomena at greater time scales to improve our understanding of the variability of coastal currents.

1 Introduction

Nearshore currents in coastal waters have a profound impact on various applications. Coastal communities rely on port operations, fisheries, and recreational tourism for economic growth and sustenance, and hence require robust infrastructure that are able to withstand strong currents (e.g. Klemas, 2011; Cervantes et al., 2015). Coastal currents also distribute nutrients, pollutants and sediment either laterally or by vertical mixing, thereby not only influencing the morphodynamics of coastal landforms such as beaches, but also the composition and health of marine ecosystems such as coral reefs and mangroves (e.g. Covey and Barron, 1988; Klemas, 2011; Xue et al., 2012; Brunner and Lwiza, 2020; Sen Gupta et al., 2021). Therefore, it is imperative to improve our understanding of the physical characteristics of coastal currents and their natural variability across time and space.

Observed current velocities are the vector sum of the tidal and nontidal components. Nontidal currents are influenced by various factors, such as meteorological forcing and local bathymetry (e.g. Chen et al., 2014; Churchill et al., 2014). Tides and tidal currents can be expressed as a linear sum of sinusoidal tidal constituents, each with a known frequency (Foreman and Henry, 1989). Harmonic analysis (HA) is traditionally used to predict and fit the amplitude and phase of each tidal constituent to the observed tidal signal (e.g. Flinchem and Jay, 2000; Pawlowicz et al., 2002). For tidal currents, the lengths of semi-major and semi-minor axes (the latter representing the direction of rotation), phase and angle of inclination, collectively known as current ellipse parameters, are estimated. Cosoli et al. (2012) used HA on two years of surface current data in the northeastern Adriatic Sea and found tidal forcing to be weak, while correlation and coherence between wind forcing and nontidal currents are high. Churchill et al. (2014) also applied HA on Red Sea coastal currents over a two-year period and likewise found tidal currents to be weak. Nevertheless, both studies acknowledged the possible contamination of tidal velocities due to diurnal wind stress. This is because one key assumption of HA is that tidal currents are stationary over the entire record length, i.e. the amplitude and phase of each tidal constituent stay constant over time (e.g. Flinchem and Jay, 2000). This assumption is often violated due to external forcing such as variable wind stress, or other internal processes such as river flow and tide–surge interaction (e.g. Horsburgh and Wilson, 2007). Moreover, as tides propagate into shallower waters near the coast, they undergo distortion which may lead to the emergence of overtides, integer multiples of fundamental tidal harmonics which are typically used to describe nonlinear interactions such as friction and advection (e.g. Zhu et al., 2021).

Over the years, a variety of spectral techniques have emerged for studying nonstationary signals. The short-term harmonic analysis (STHA) involves conducting HA on short consecutive segments of the entire time series to provide moderate localisation of events involved in the modulation of tidal processes (Jay and Flinchem, 1995). Dusek et al. (2017) performed bimonthly HA on an 11-year record of estuarine currents in Tampa Bay, Florida, and found that tidal currents strengthen during periods of strong land–sea breeze and high freshwater discharge. However, STHA cannot resolve constituents with periods longer than the window length nor capture the temporal variation of tidal constituents (Flinchem and Jay, 2000). In contrast,

the wavelet transform uses a finite function with translation and scaling parameters, also known as the mother wavelet, to build a class of functions with a finite integrated squared value (e.g. Flinchem and Jay, 2000). Specifically, the continuous wavelet transform (CWT) uses an arbitrary number of these basis functions to convert the time-series into two-dimensional plots of time and frequency, providing improved localisation of events (e.g. Jay and Flinchem, 1995; Torrence and Compo, 1998; Flinchem and Jay, 2000; Hoitink and Jay, 2016). However, the CWT is limited to extracting information on tidal species across different frequency bands instead of examining specific tidal constituents such as M_2 and K_1 due to the time–frequency trade-off governed by the Heisenberg uncertainty principle (Torrence and Compo, 1998; Flinchem and Jay, 2000). Additionally, to measure the cross-correlation between two CWT, the magnitude-squared wavelet coherence (WC) is calculated (Grinsted et al., 2004).

The application of CWT is common in the study of estuarian dynamics. Jay and Flinchem (1995) revealed stronger semidiurnal and quarterdiurnal tidal signals during the generation of plume internal tides in the Columbia River Estuary, though their relationships with physical mechanisms remain ambiguous. Analysing the CWT of currents has also yielded insights on how seasonal river discharge influences tidal damping and the modulation of shallow water constituents in the Mahakam River in Indonesia (Sassi and Hoitink, 2013), the Yangtze River Estuary in China (Guo et al., 2015), and the Guadalquivir River Estuary in Spain (Losada et al., 2017). Zaytsev et al. (2010) employed both HA and rotary-multiple filter technique, the equivalent of CWT, and found persistent intense counterclockwise rotary currents presumably driven by counterclockwise sea breeze winds in the Bay of La Paz, Mexico. Currents have a greater propensity to nonstationary interactions than water levels and thus should not be overlooked (Guo et al., 2015). However, the relationship between currents and other drivers remains unclear, with local wind forcing having substantial impact on surface current variability (Ursella et al., 2006).

With this in mind, we aim to explore the nonstationary behaviour of coastal currents and their various drivers, with a focus on the Singapore Strait. The Singapore Strait links the South China Sea (SCS) and the Malacca Strait and is one of the busiest shipping routes in the world (e.g. Chen et al., 2005; Hasan et al., 2012). It has also undergone extensive development such as land reclamation and shore protection work that has majorly altered shoreline configuration and inevitably impacted local hydrodynamics. In the Singapore Strait, tidal asymmetry exists since tides transition from predominantly diurnal in the east to semidiurnal in the west (Chen et al., 2005; Tkalich et al., 2013), hence tides are semidiurnal while currents are mostly diurnal (Van Maren and Gerritsen, 2012; Peng et al., 2023). The tidal asymmetry is further complicated by the complex bathymetry as many islands such as rock outcrops and coral reefs lie within the strait (Chen et al., 2005; Hasan et al., 2012). As depicted in Figure 1, the Singapore Strait has a highly variable bathymetry of up to 100 m in depth, with deeper depths of up to 200 m recorded near Kusu Island. Additionally, the hydrodynamics are affected by local wind systems. Yearly, Singapore experiences two monsoon seasons with two inter-monsoons in between: the northeast (NE) monsoon from mid-November to March when northeasterly winds blow across the SCS, and the southwest (SW) monsoon from mid-May to mid-September when wind circulation reverses (Van Maren and Gerritsen, 2012; Martin et al., 2022). The stronger and longer NE monsoon results in

currents flowing net westward along the hydrodynamic pressure gradient from the SCS out to the Malacca Strait and Java Sea and only reverses in direction during the SW monsoon (Chen et al., 2005; Van Maren and Gerritsen, 2012; Martin et al., 2022). The monsoons generally exhibit variability on different time scales from intraseasonal to interannual, the former strongly influenced by the Madden-Julian oscillation (MJO), and the latter by the El Niño Southern Oscillation (ENSO) (Robertson et al., 2011).

Due to a lack of long-term observational records from Singapore, local hydrodynamics are typically modelled at coarse resolution and predicted using numerical models. Three-dimensional models have been used to simulate tidal currents in the Singapore Strait (e.g. Chen et al., 2005; Zhang, 2006), and further refined by expanding the grid boundaries (Hasan et al., 2012; Van Maren and Gerritsen, 2012) and incorporating multi-scale nesting to improve grid resolution (Hasan et al., 2016). These models were forced by major tidal constituents and did not include wind forcing due to heavy computational demands, thereby making the study of hydrodynamics in the Singapore Strait especially challenging. Nevertheless, such studies are crucial given their potentially significant implications on port operations, coastal sediment dynamics, and larval connectivity of marine ecosystems. In particular, sedimentation of fine-grained sediment is chronic within Singapore Strait, and it influences the distribution and growth of coral reef communities. Here we focus on two coral reef platforms located within southern Singapore: Pulau Hantu (1.226247° N, 103.747049° E) and Kusu Island (1.225354° N, 103.860104° E) (Fig. 1). These fringing coral reefs are consistently subjected to high turbidity and sedimentation, as well as significant nearshore current velocities (Morgan et al., 2020). We used a one-year time-series of current velocity and direction data to achieve the following objectives: (1) analyse the general properties of currents and their ellipse parameters using harmonic analysis, (2) investigate the time-averaged properties of wind stress, (3) estimate the power spectral density (PSD) of currents in the Singapore Strait by partitioning the variance into four frequency bands and quantify the contribution of tides, (4) examine how the spectral properties of both currents and wind vary with time using CWT, and (5) evaluate their relationship using WC, complemented with the results of STHA. The structure of the paper is as follows: Sect. 2 covers the type of data collected and the methods employed to achieve the study objectives. The results of the study are described and discussed in Sect. 3 and Sect. 4 respectively. Lastly, conclusions are given in Sect. 5.

2 Data and Methods

2.1 ~~Field d~~Data collection

The bathymetry data of Singapore shown in Figure 1 has a 25 m resolution and were compiled from several sources: the Hydrographic and Nautical Charts from Navionics Webapp (Navionics, 2023), the General Bathymetric Chart of the Oceans at a 15 arc-second resolution (GEBCO Compilation Group, 2023), the 10 m Digital Terrain Model from the Singapore Land Authority (SLA, 2019), and the 30 m Shuttle Radar Topography Mission data (NASA JPL, 2013). The land boundaries of

Malaysia and Indonesia were obtained from Hijmans and University of California (2015) and the Humanitarian Data Exchange (n.d.) respectively.

At Pulau Hantu and Kusu Island, we each deployed four Tilt Current Meters (TCM: TCM-1 Lowell Instruments) following
130   the main compass axes of the reefs (north, south, east and west) (Fig. 1). TCMs operate by the drag-tilt principle, in which the meter tilts in the direction of the drag of the fluid. To minimise the effects of vortex eddies, turbulence and waves, the TCM was configured to record data at 8 Hz for 15 seconds (i.e. 160 samples) per minute and the data is burst-averaged over each minute (Lowell et al., 2015). The accuracy specifications of TCMs for speed and direction respectively are 3 cm s^{-1} + 3 % of reading and 5° for current speeds exceeding 5 cm s^{-1}. We collected data on speed, direction, zonal (u-) and meridional (v-)
135   velocities at a 10-minute sampling interval at a shallow depth of ~3 m from March 2018 to March 2019, except Hantu North where data were collected until December 2018 due to instrument malfunction. From the 51,000 data observations, there were eight and seven consecutive missing data points in Hantu West and Kusu South, respectively. Since data needs to be continuous for wavelet analysis, we interpolated the missing data using a moving median with a window length of 2 hours.

140
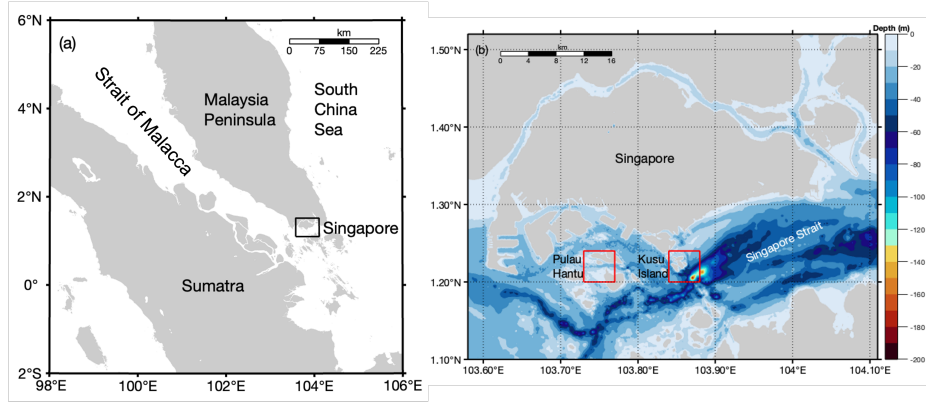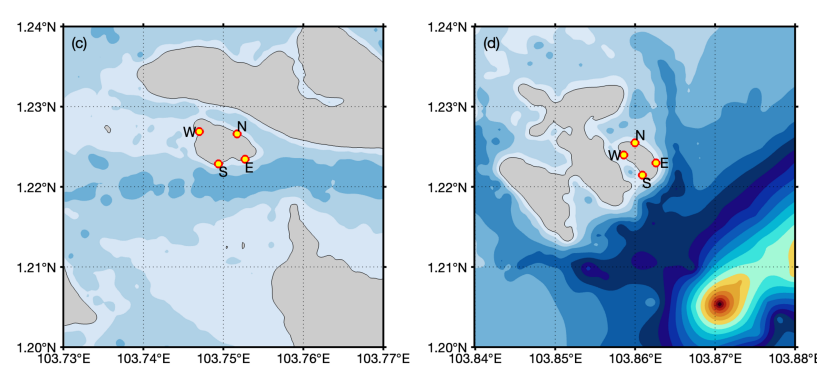
Figure 1. (a) A map of the Southeast Asia region (Amante and Eakins, 2009) with Singapore indicated by the black rectangle. (b) A zoomed-in map of Singapore with the location of our study areas, Pulau Hantu and Kusu Island, in the southern coast of Singapore (indicated by the red rectangles). The background colour represents the bathymetry (GEBCO Compilation Group, 2023; Navionics, 2023). (c) A zoomed-in map of Pulau Hantu with the four study sites, where the TCMs are deployed, being marked by yellow circles and labelled according to their compass bearings, and (d) likewise for Kusu Island.

To examine the role of local winds, we obtained dynamically downscaled hourly zonal and meridional wind velocity data from the Tropical Marine Science Institute in Singapore. Dynamical downscaling was performed using the Weather Research and Forecasting (WRF) model version 4.4.1 (Skamarock et al., 2019). The WRF model was setup with a horizontal grid of 10 km resolution covering Southeast Asia and centred at a point with coordinates 8.5°N and 115°E, and then forced by ERA5 atmospheric reanalysis data, whose horizontal resolution is 0.25° x 0.25° or about 31 km (Hersbach et al., 2020). We extracted the wind data from the grid points closest to both islands and used the drag coefficients from (Large and Pond, 1981) to derive wind stress from wind velocities at 10 m reference height.

2.2 Analysis methods

We first performed Principal Component Analysis (PCA) to resolve both currents and wind stress, initially expressed as eastward and northward vectors, into uncorrelated orthogonal components with their mean value subtracted. PCA is useful for analysing highly directional variables such as coastal currents, which generally flow parallel to the coastline. Therefore, its alongshore and cross-shore current can be defined by the major and minor axis component respectively, the former which accounts for most of the total variance (Thomson and Emery, 2014). We then performed harmonic analysis on currents at each site over the entire observation period using the MATLAB UTide package (Codiga, 2011) to extract the current ellipse

parameters of major tidal constituents. Additionally, we calculated the hourly and monthly wind stress averages of both Pulau Hantu and Kusu Island to examine the variation across different periods.

165 Using the MATLAB toolbox "jLab" (Lilly, 2019), we chose a time-bandwidth product of 3 and 13 Slepian tapers to obtain multi-taper PSD estimates of currents and wind. This method provides a smoother estimate of the spectrum than the traditional Fourier transform as the spectrum is an average of multiple independent spectra estimates that are generated from the same sample, thereby minimising spectral leakage (Percival and Walden, 1993). The sampling rate for both currents and wind stress converts to a Nyquist frequency of 72 cycles per day (cpd) and 12 cpd respectively. We visually inspected the spectra for any
170 peaks and gaps before partitioning the variance into 4 frequency bands: low-frequency, $f < 0.72$ cpd; diurnal, $f = 0.72–1.5$ cpd; semidiurnal, $f = 1.5–2.3$ cpd; and high-frequency, $f > 2.3$ cpd. Diurnal and semidiurnal frequencies hereafter will be collectively referred to as tidal frequencies. We then quantified the variance by integrating the spectrum over each frequency band via rectangle approximation and expressed the relative contribution as a percentage of the total variance. The 95 % confidence intervals for spectral estimates were calculated assuming a χ^2 distribution of variance.
175

Wavelet analysis was done with the MATLAB toolbox "Cross wavelet and wavelet coherence" (Grinsted, 2023). To analyse the time series at different periods or frequencies, the wavelet is scaled accordingly and translated in time. We selected the Morlet wavelet as it is optimal for processing tidal signals, 12 scales per octave, and a dimensionless frequency of 6 to provide a good balance between time and frequency resolution (Torrence and Compo, 1998; Grinsted et al., 2004). The wavelet power
180 is normalised by the variance of the time series, and the cone of influence (COI) demarcates the area where edge effects cannot be ignored (Grinsted et al., 2004). Edge effects typically arise when the wavelet is stretched and located near the start and end of the data because it extends outside the boundary of the time series. Therefore, information that lies outside the COI should be treated with caution.

185 Finally, we used WC to examine the strength and phase of the localised correlation between currents and wind stress. The arrows in WC analysis represent the relative phase or the time lag between both variables, with the level of statistical significance estimated using Monte Carlo methods (Grinsted et al., 2004). The time lag at a specific period is calculated as the phase angle divided by 2π times the period and requires careful interpretation. For instance, arrows pointing to the left represents an anti-phase relationship, which could either indicate negative correlation or one variable leading the other by half
190 the period. An in-phase relationship means that the relative phase is 0° with arrows pointing to the right. We complemented WC with STHA to observe for any similar trends. We ran STHA through the MATLAB toolbox UTide (Codiga, 2011) using a 60-day window and moved with a time step of 1 day to provide seasonal resolution while maintaining result accuracy. A bimonthly window also resolves 35 tidal constituents, including those with longer periods up to monthly such as M_m, and in this case constituents with similar frequencies N_2 and M_2.

195 **3 Results**

3.1 General characteristics of currents

From the PCA results, the alongshore current accounts for 67 % to 87 % of current variance in most study sites but only 54 % in Hantu West (Table 1). This could be attributed to the slightly concave nature of the coastline of Hantu West and hence flow is not strictly rectilinear. Mean and maximum current speeds across the time-series were also calculated for each site. Within

200 the time domain, the mean speed of currents at the Pulau Hantu sites ranged from 9.3–19.6 cm s^{-1} with maximum speeds of up to 119.8 cm s^{-1} (Table 1, Fig. 2). Currents at the Kusu Island sites are generally weaker throughout the duration with mean speeds ranging from 6.7–14.7 cm s^{-1} (Table 1). Sites situated at the east and west of both islands experience higher mean speeds of 11.6–19.6 cm s^{-1}, as compared to the north and south sites where mean speeds are weaker and do not exceed 10 cm s^{-1} (Fig. 2). During the spring tides, current speeds more than quadrupled from about 20 cm s^{-1} to about 100 cm s^{-1} consistently

205 at both Hantu East and Hantu West. However, at Hantu North, Hantu South, and Kusu West, the increase in speed is less consistent, also reaching up to about 100 cm s^{-1}, but only during 5 periods of spring tide every month during the monsoon seasons from May to September and from December to March. At Kusu South, currents exceeded 40 cm s^{-1} only in Mar–Apr 2018 and remain weak over time. Kusu East and Kusu North exhibit consistent temporal variation, with the former recording slightly greater speeds during the NE monsoon.

210

Table 1. Properties of the principal components of currents.

Site	PC1 (%)	PC2 (%)	Positive direction		Mean speed (cm s^{-1})	Mean current direction (°)	Max current speed (cm s^{-1})
			PC1	PC2			
Pulau Hantu							
North	82.7	17.3	SE	NE	9.3	143.2	109.0
South	68.4	31.6	NE	NW	9.7	288.1	115.4
East	67.2	32.8	NE	NW	19.6	253.3	119.8
West	53.8	46.2	NW	NE	12.5	38.9	119.8
Kusu Island							
North	87.1	12.9	SE	NE	7.9	274.4	34.1
South	85.0	15.0	NW	NE	6.7	143.5	90.1
East	85.9	14.1	NW	NE	14.7	160.9	62.8
West	74.7	25.3	NW	NE	11.6	325.7	119.6
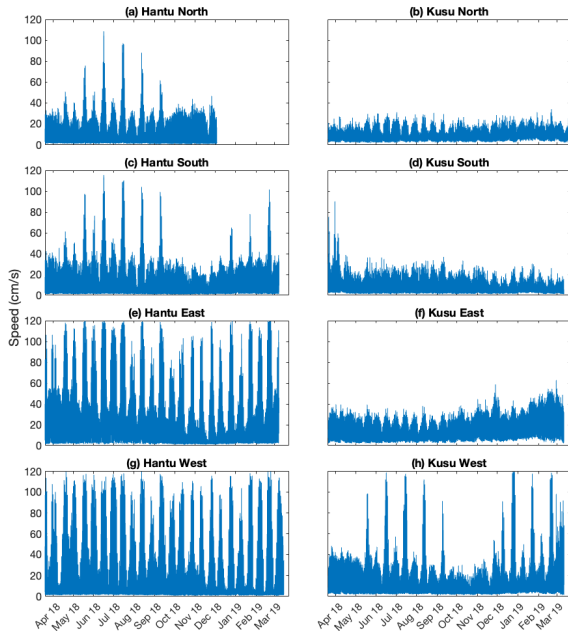
Figure 2. Current speeds over time at (a) Hantu North, (b) Kusu North, (c) Hantu South, (d) Kusu South, (e) Hantu East, (f) Kusu East, (g) Hantu West and (h) Kusu West.

Current ellipses for the major tidal constituents were calculated using harmonic analysis and presented in Figure 3. The amplitudes of the ellipses are greater at the east and west sites of both Pulau Hantu and Kusu Island, which meant stronger
220 currents in those areas, while the amplitudes at Kusu South are the lowest. The eccentricity of the ellipses, which can be loosely defined as the ratio of the semi-minor axis length to the semi-major axis length, is very low across most sites and thus indicates a rectilinear flow along the coastlines, while the ellipses at Hantu West are slightly rotund. Such results align well with the earlier analysis. In addition, the diurnal tidal currents are generally more dominant, as seen from the larger K_1 and O_1 amplitudes, while the semidiurnal M_2 currents are only strong in Hantu East and Hantu West. M_2 currents are much stronger
225 than S_2 currents, and the amplitude of P_1 currents compared to the main diurnal constituents are very small. It should be emphasised that the current ellipses, while useful in displaying the strength and orientation of currents, do not include any information about the non-stationary behaviour of currents and thus should be complemented with extra techniques outlined in the previous section.

230
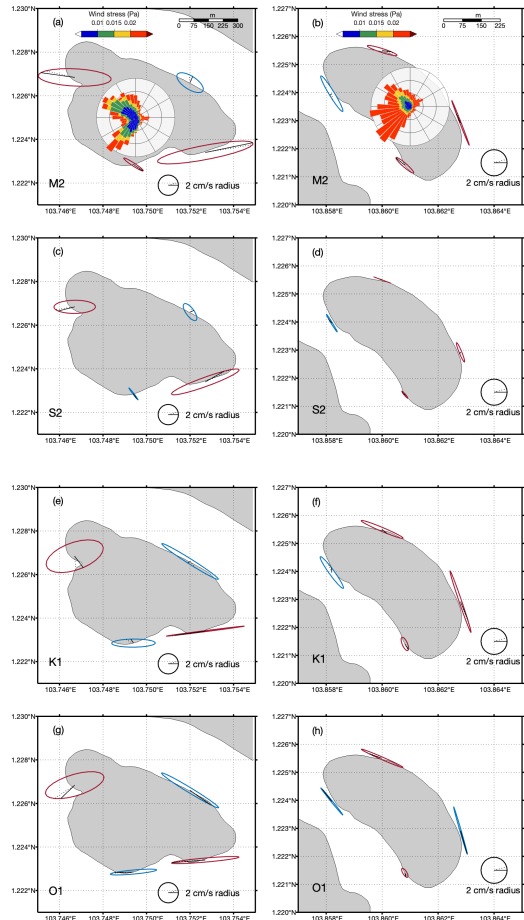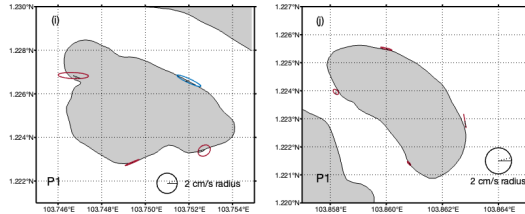
Figure 3. Tidal current ellipses for M_2 [(a), (b)], S_2 [(c), (d)], K_1 [(e), (f)], O_1 [(g), (h)], and P_1 [(i), (j)] at all study sites in Pulau Hantu (left column) and Kusu Island (right column). Ellipses are depicted in red if they show a counterclockwise movement. Wind roses for wind stress from March 2018 to March 2019 at (a) Pulau Hantu, and (b) Kusu Island.

3.2 General characteristics of wind stress

The major axis wind stress over Pulau Hantu and Kusu Island account for 61 % and 77 % of the wind variance respectively and blow predominantly to the southeast from the SCS, with Kusu Island recording stronger winds (Table 2). These winds strengthen during December to March and are thus representative of the NE monsoon. In contrast, the wind direction of minor axis winds is directed north-westward and become stronger from June to September, thereby coinciding with the SW monsoon. The wind rose for both Pulau Hantu and Kusu Island provides a good visualisation of the strength and directionality of the winds. (Fig. 3).

Table 2. Properties of the principal components of wind stress.

Site	PC1 (%)	PC2 (%)	Positive direction PC1	Positive direction PC2	Mean wind stress (Pa)	Mean wind stress direction (°)
Pulau Hantu	60.7	39.3	NE	NW	0.0149	280.4
Kusu Island	76.9	23.1	NE	NW	0.0296	252.5

Wind stress was averaged for both Pulau Hantu and Kusu Island over each hour of the day (Fig. 4a). The average wind stress along both principal components is diurnal and asymmetric, characteristic of the land-sea breeze circulation in Singapore. The northeast and northwest directions are taken to be positive for the major and minor axis respectively (Table 1). During the day, averaged wind stress is directed north and reverses in direction at night, with maximum magnitudes of the major axis winds occurring at about 13:00 and 20:00 local time respectively at Pulau Hantu. The maximum major axis wind stress during the day at Kusu Island occurs slightly earlier at about 11:00 local time. Owing to differential heating between the land and sea, the sea breeze blowing northward from the Singapore Strait during daytime is usually stronger than the land breeze coming from the Malay Peninsula late at night (Li et al., 2016). Interestingly, the diurnal pattern is more pronounced from about June to

November, which comprises of the SW monsoon and the following inter-monsoon period, where the averaged wind stress
increases in strength and directed northward as seen from the monthly-averaged plot (Fig. 4b). Likewise, we can infer the daily
variation of averaged wind stress during the NE monsoon and the following inter-monsoon period, from about December to
April, is a predominantly southward orientation that is most intense at night (Fig. 4b).
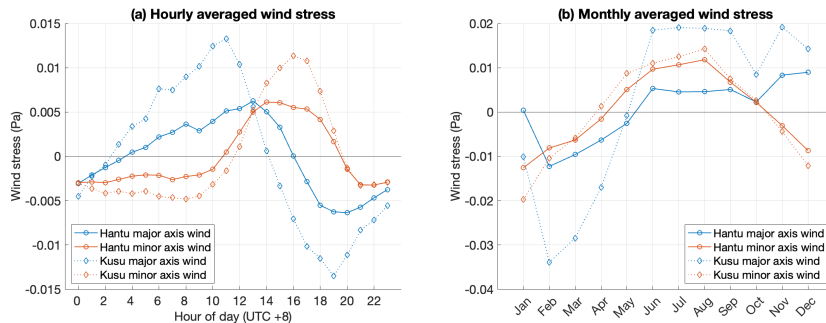
Figure 4. Wind stress of Pulau Hantu and Kusu Island with their respective principal axis, averaged over (a) hour of day, and
(b) month of year.

3.3 Power spectral density

We calculated the PSD to partition the variance into frequency bands and quantified them for both alongshore and cross-shore
currents. Here we can observe that spectral peaks are most prominent at tidal frequencies, with diurnal currents being slightly
stronger than semidiurnal currents (Fig. 5). The spectra yield two distinct peaks within the diurnal band, which correspond to
the major diurnal tidal constituents K_1 (1.0032 cpd) and O_1 (0.9288 cpd). Higher frequency signals from the third diurnal to
the eighth diurnal bands are also discernible, though not as strong as currents oscillating at tidal frequencies. Meanwhile, only
the fortnightly signal is significant within the low-frequency band, which could represent the lunisolar synodic fortnightly tidal
constituent MS_f. The MS_f constituent illustrates spring–neap variations caused by quadratic nonlinear interactions of the M_2
and S_2 tidal constituents (Hoitink and Jay, 2016). Wind stress spectra also show the presence of a strong land–sea breeze,
evidenced by the sharp and narrow peaks occurring at periods of about 24 and 12 hours, the latter to a smaller extent.
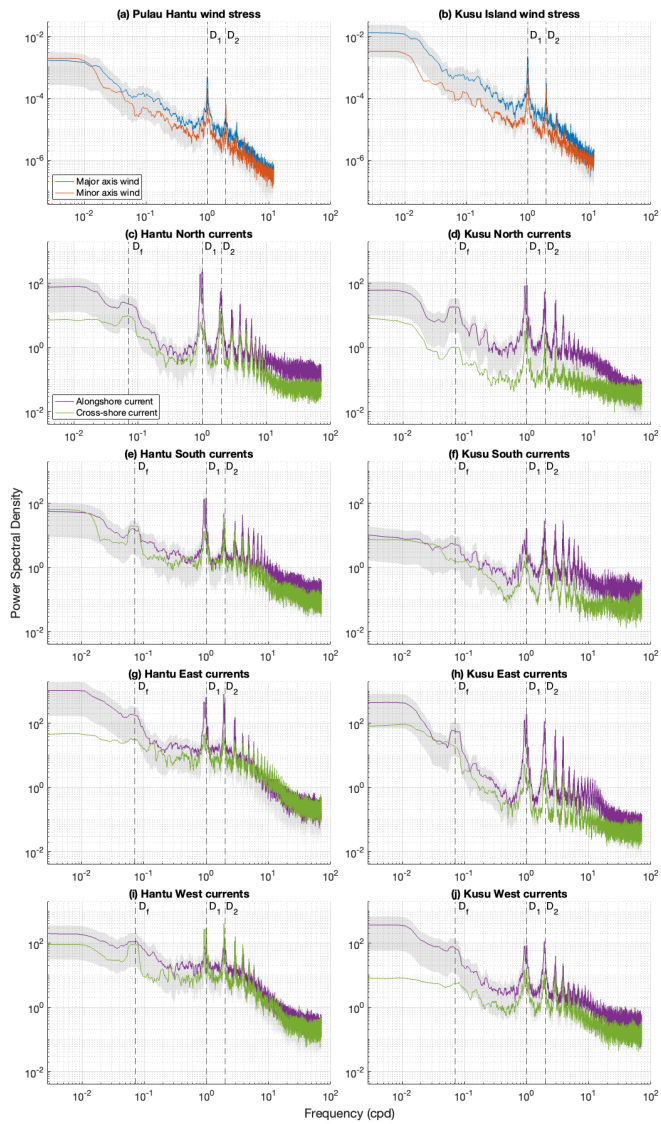
Figure 5. Power spectral density estimates of both major and minor axes wind stress in (a) Pulau Hantu and (b) Kusu Island, with units of Pa^2 cpd^{-1}, as well as that of both alongshore and cross-shore currents recorded at (c) Hantu North, (d) Kusu North, (e) Hantu South, (f) Kusu South, (g) Hantu East, (h) Kusu East, (i) Hantu West and (j) Kusu West, with units of cm^2 s^{-2} cpd^{-1}. The shading indicates the 95 % confidence level for the major axis wind stress and alongshore currents. The vertical dashed black lines loosely represent (from left) the fortnightly (D_f) shown only in the currents plots, diurnal (D_1), and semidiurnal (D_2) frequency bands.

Table 3 presents the ~~quantification of~~ total velocity variance, which is the sum of the variances of low-frequency (LF), diurnal (D), semidiurnal (SD), and high-frequency (HF) bands, and the variances of LF, D, and SD motions. The variance of alongshore and cross-shore currents, denoted by PC1 and PC2 respectively, for each frequency band are also shown. ~~for each frequency band.~~ The ~~computed~~total percentage variance of ~~alongshore and cross-shore currents, denoted by~~ PC1 and PC2 currents~~respectively,~~ are similar to the PCA results shown in Table 1. Tidal frequencies are responsible for about 26–45 % and 14–36 % of the total current variance across all sites in Pulau Hantu and Kusu Island respectively, with the spectral energy of diurnal currents being at least 1.3 times higher~~stronger~~ than semidiurnal currents in Hantu North, Hantu South, Kusu North, and Kusu East (Table 3). ~~High frequency motions, which consist of mainly overtides, are depicted in the peaks from the third to eighth diurnal frequency bands, which further attest to the chaotic behaviour of tidal motions occurring near the coasts.~~

Table 3. Variance (in cm^2 s^{-2}) of the filtered currents obtained from PSD. The variance for each frequency band is calculated by integrating the spectrum using rectangle approximation, with the relative contribution expressed as a percentage of the total variance. The variance of high-frequency currents is not shown here.

Site	Frequency band											
	Low-frequency (LF)			Diurnal (D)			Semidiurnal (SD)			Total (LF+D+SD+HF)		
	PC1	PC2	Total	PC1	PC2	Total	PC1	PC2	Total	PC1	PC2	Total
Pulau Hantu												
North	4.3	1.1	5.4	20.1	1.2	21.3	7.9	1.7	9.6	56.9	11.7	68.6
%	6.3	1.6	7.9	29.3	1.7	31.0	11.5	2.5	14.0	82.9	17.1	100.0
South	3.7	2.9	6.6	12.4	2.5	14.9	5.0	3.1	8.1	63.7	25.8	89.5
%	4.1	3.2	7.4	13.9	2.8	16.6	5.6	3.5	9.1	71.2	28.8	100.0
East	46.5	8.6	55.1	58.7	11.1	69.8	64.3	11.0	75.3	249.5	98.1	347.6
%	13.4	2.5	15.9	16.9	3.2	20.1	18.5	3.2	21.7	71.8	28.2	100.0
West	24.4	10.9	35.3	21.7	25.7	47.4	28.5	25.8	54.3	172.1	128.8	300.9
%	8.1	3.6	11.7	7.2	8.5	15.8	9.5	8.6	18.0	57.2	42.8	100.0

Kusu Island

North	2.9	0.3	3.2	7.8	0.5	8.3	4.8	0.2	5.0	32.0	4.6	36.6
%	7.9	0.8	8.7	21.3	1.4	22.7	13.1	0.5	13.7	87.4	12.6	100.0
South	1.1	0.6	1.7	1.8	0.4	2.2	2.8	0.6	3.4	32.2	7.2	39.4
%	2.8	1.5	4.3	4.6	1.0	5.6	7.1	1.5	8.6	81.7	18.3	100.0
East	12.2	3.8	16.0	13.9	0.7	14.6	10.3	0.6	10.9	59.6	10.3	69.9
%	17.5	5.4	22.9	19.9	1.0	20.9	14.7	0.9	15.6	85.3	14.7	100.0
West	14.7	1.4	16.1	11.9	2.4	14.3	14.9	2.2	17.1	95.7	26.3	122.0
%	12.0	1.1	13.2	9.8	2.0	11.7	12.2	1.8	14.0	78.4	21.6	100.0

3.4 Continuous wavelet transform of currents and wind stress

The CWT of alongshore and cross-shore currents at all study sites show that the diurnal and fortnightly signals are strongest and statistically significant (Fig. 6 and Fig. S1 in Supplementary material). In addition, energetic semidiurnal and monthly signals are also present. Strong alongshore currents at tidal frequencies occur about twice a month, which incidentally coincided with the spring–neap tidal cycle. The presence of statistically significant regions in Hantu West is better observed in the CWT of its cross-shore currents (Fig. S1), where there is minimal spectral leakage and currents are strongest at tidal and fortnightly frequencies. High frequency oscillations are also present all-year round, highlighting the chaotic nature of currents flowing near the coasts. The wavelet power is generally negligible between the period of 1 to 8 days. In addition, strong low-frequency currents are detected at a periodicity of about 32 days (Fig. 5 and Fig. S1 in Supplementary material), which likely indicates the presence of intraseasonal variability.

Nonstationary behaviour of currents is clearly exhibited as the wavelet power across frequency bands show significant temporal variation. Alongshore currents are unusually weak during the inter-monsoon period from September to October in Hantu East, Hantu South and Kusu West, with Kusu West showing the greatest contrast (Fig. 6). At Kusu East and Kusu North, diurnal currents seem to intensify when the NE monsoon begins in December, which contrasts with Kusu South where currents at tidal frequencies are heavily attenuated from November onwards (Fig. 6).
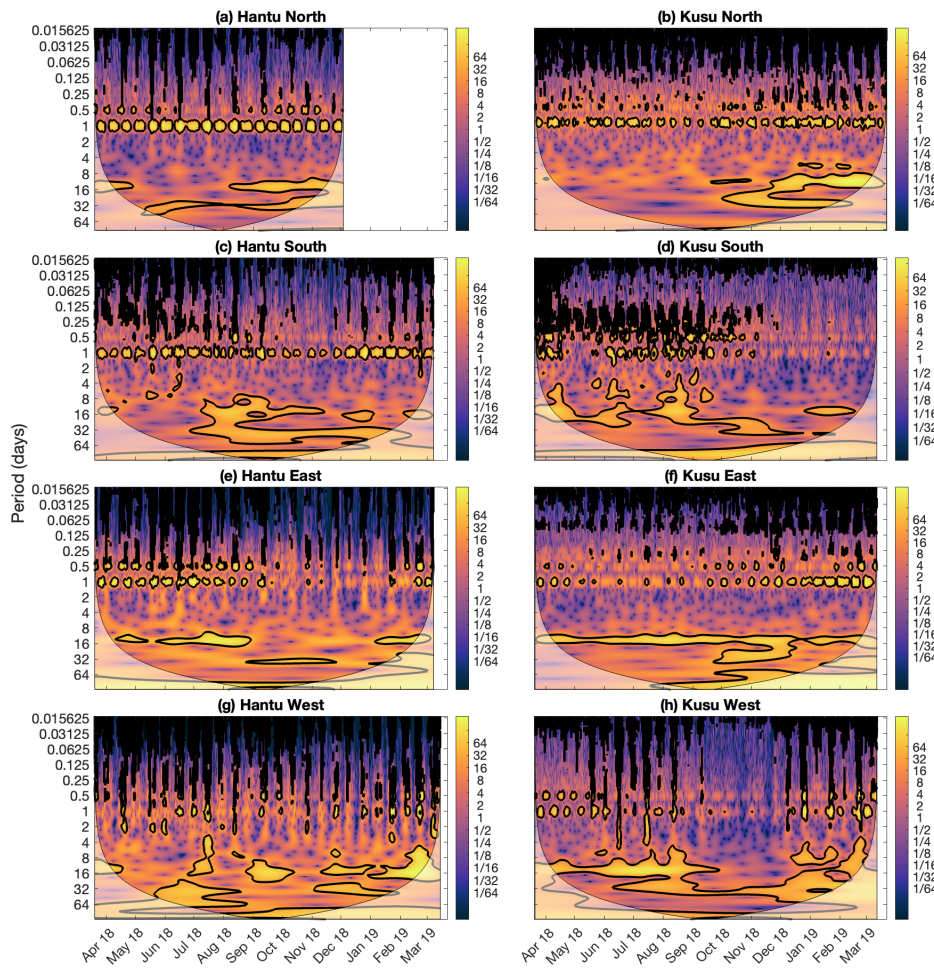
Figure 6. CWT of alongshore currents at (a) Hantu North, (b) Kusu North, (c) Hantu South, (d) Kusu South, (e) Hantu East, (f) Kusu East, (g) Hantu West and (h) Kusu West. The thick black contour encompasses significant regions against red noise ($p < 0.05$), and the cone of influence (COI) is shown as a lighter shade where edge effects cannot be ignored. The wavelet power is $\log_2(A^2\,v^{-1})$, where A is the wavelet amplitude, and v is the variance of the entire signal.

The CWT of wind stress present powerful and statistically significant oscillations at the diurnal and monthly frequencies (Fig. 7). Diurnal wind stress is strongest during the NE monsoon from December to March. The minor axis diurnal wind stress at Pulau Hantu, while not as strong during the NE monsoon, recorded considerable strength in the months from June to October, the period when the SW monsoon regime is dominant. Similar to the CWT of currents, the low-frequency winds are strongest in periods of about 32 days from December to February for Pulau Hantu, and from April to October for Kusu Island, which suggests strong periods of MJO activity.
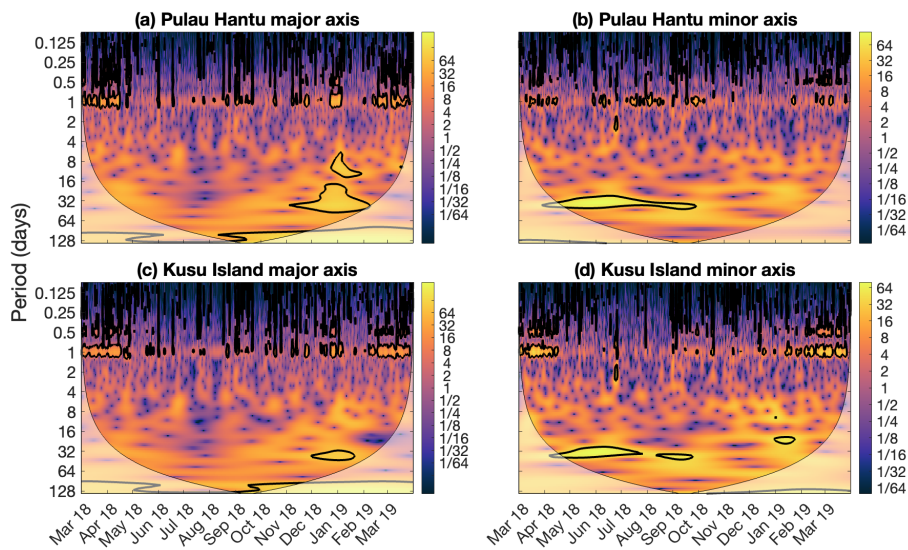
Figure 7. CWT of wind stress at (a) Pulau Hantu major axis, (b) Pulau Hantu minor axis, (c) Kusu Island major axis, (d) Kusu Island minor axis.

3.5 Wavelet coherence between currents and wind stress, and STHA of currents

The WC between both alongshore currents (Fig. 8) and cross-shore currents (Fig. S2 in Supplementary material) and major axis wind stress reveal strong correlation over a broad range of frequencies, with the low and diurnal frequency bands being the most significant. The arrows represent the phase relationship between both variables; arrows pointing upwards with respect to the phase indicates that currents are leading wind stress, and vice versa.

At periods of 32 days or longer, correlation from September onwards is high, significant, and largely in phase at most sites. This suggests that the MJO plays a significant role in modulating the intraseasonal variability of coastal currents. At Kusu North and Kusu South, the phase difference of 30° indicates that the currents lead the winds by a few days. However, at Hantu North and Kusu East, the relative phase is approximately 90–120° pointing down, which means that strong currents occur about 1 to 2 weeks later.

At the diurnal frequency band, correlation was generally significant, albeit rather sporadically, during the monsoon seasons for most sites. This suggests that nontidal processes such as wind stress introduces nontidal energy at tidal frequencies (Pugh, 1987). In addition, the relative phase relationship has considerable temporal and spatial variability. Correlation is weak and close to zero during the inter-monsoon from September to November, albeit with short periods of high correlation in between (Fig. 8 and Fig. S2). During the SW monsoon from June to September, correlation between the major axis wind stress and alongshore currents is high and approximately in phase at Hantu East, Hantu South, Kusu East and Kusu North (Fig. 8), with a phase angle at Kusu East of about 0–90° pointing down. This corresponds to wind stress leading currents by up to 6 hours. In contrast, the correlation at Hantu North is almost anti-phase. Considering the NE monsoon, statistically significant regions are observed in Hantu East, South, Kusu East, North and West. The correlation is approximately in-phase at Kusu West and anti-phase at Hantu East and Kusu East, while the phase relationship at Hantu South and Kusu North is highly variable with the phase angle fluctuating wildly from 0–270° with respect to the phase. As such, it is not immediately clear whether the currents or wind stress is the leading variable.
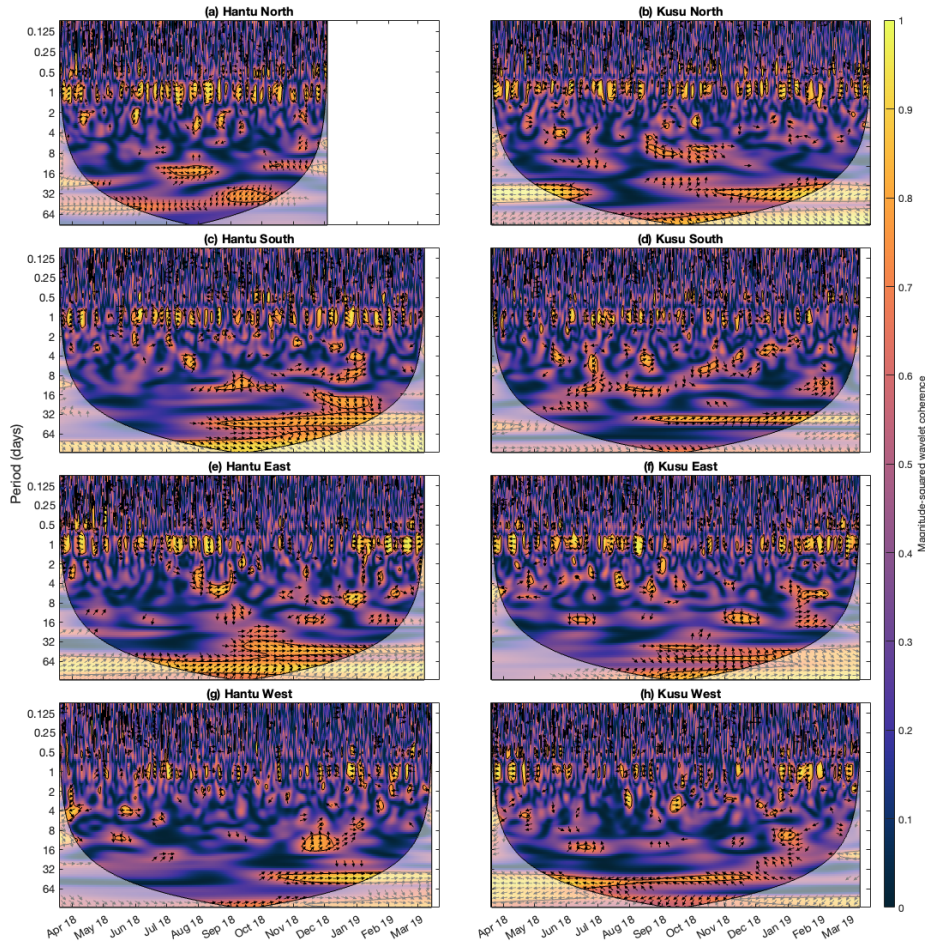
Figure 8. Wavelet coherence between alongshore currents and major axis wind stress at (a) Hantu North, (b) Kusu North, (c) Hantu South, (d) Kusu South, (e) Hantu East, (f) Kusu East, (g) Hantu West and (h) Kusu West. The black contours indicate significant regions and the cone of influence (COI). The area that lies outside the COI has a lighter shade and information in this area should be treated with caution. The arrows represent the relative phase relationship, with arrows pointing right and left indicating in-phase and antiphase respectively, and winds leading currents by 90° pointing down.

350

355

We presented the semi-major axis amplitude of four main tidal constituents K_1 (Fig. 9), O_1, M_2, and S_2 (Figs. S3–S5 respectively in Supplementary material). Though the amplitudes of most major tidal constituents are generally large, they do not seem to exhibit any trend. However, except for Kusu South where currents are generally very weak, the amplitude of the

360   K_1 tidal constituent appeared to vary semi-annually and ranges from about 1 to 18 cm s^{-1} during the monsoon seasons. In Pulau Hantu, the K_1 amplitude is generally greater than that in Kusu Island, which is not surprising since currents in Pulau Hantu are generally stronger. This suggests that diurnal wind forcing amplified during the monsoon seasons could result in a corresponding increase of the K_1 amplitude of currents.
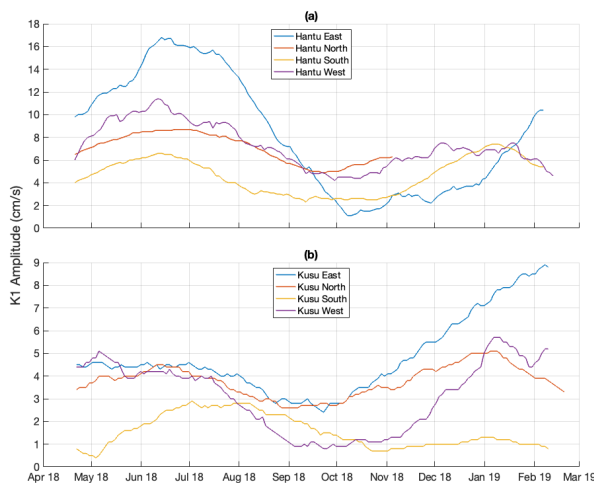
365   **Figure 9.** K_1 tidal amplitudes of all sites in (a) Pulau Hantu and (b) Kusu Island, derived from STHA.
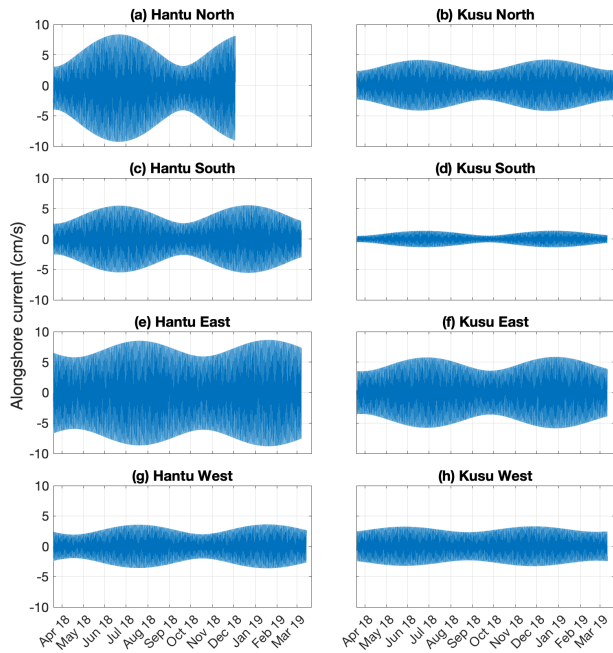
Figure 10. Reconstructed alongshore current velocities using only P_1 and K_1 tidal constituents.

4 Discussion

370 The high correlation displayed in the coherence analyses indicates the significance of wind forcing in driving currents at various time scales. Low-frequency winds in the tropics are dominated by the MJO, a period of 30–90 days defined by the eastward propagation of deep atmospheric convection and anomalous rainfall in the Tropical Pacific (Madden and Julian, 1971; Zhang, 2005). Hu et al. (2023) discovered that as the MJO crossed through the Maritime Continent during the winter months from November to March, there was an eastward anomalous subsurface warm current in the Timor Sea propagating

375 ahead of the MJO convection centre due to a deeper thermocline excited by the wind field anomalies. Likewise, the generation of MJO convection in the later months of the year creates persistently strong coastal currents in Pulau Hantu and Kusu Island that could help in sustaining the MJO propagation.

Diurnal currents are stronger than semidiurnal currents (Fig. 7) due to the presence of an amphidromic point for the main diurnal constituents in the Singapore Strait (Pugh, 1987). Van Maren and Gerritsen (2012) further deduced that the K_1 tide is a standing wave as it propagates from the SCS and reflects off the Sumatra coast, generating high velocities in the Singapore Strait that are predominantly diurnal despite Singapore experiencing a semidiurnal tidal regime. To add on, only the K_1 currents exhibit semi-annual variation, with amplitudes increasing during the monsoon seasons (Fig. 9). It is not uncommon to observe seasonal modulation in tides and tidal currents, particularly in shallow waters where there are seasonal changes in stratification. During the summer when there is less mixing in the water column, there is reduced vertical eddy viscosity and energy loss, leading to higher tidal amplitudes and hence stronger currents (Müller, 2012). For instance, the amplitude of the M_2 tide and tidal currents are larger during the summer in the East China and Yellow Seas (Kang et al., 2002), and the Bohai Sea (Wang et al., 2020). However, Singapore's water column is generally fully mixed with minor stratification during neap tides (Hasan et al., 2013). We then postulated that other mechanisms such as interaction between tidal constituents and meteorological forcing are responsible for the seasonal modulation of K_1 currents. For example, seasonal tidal variations are coherent with the western North Pacific monsoon index in Southeast Asia (Devlin et al., 2018), and with ENSO in the Soloman Islands (Devlin et al., 2014).

We used the results of harmonic analysis to reconstruct alongshore current velocities using only K_1 and P_1 constituents. Although the amplitude of P_1 is much smaller than K_1 (Fig. 3), their interaction results in a pronounced semi-annual variation of about 183 days, the inverse of the difference in their frequencies (Fig. 10). This phenomenon is also observed in diurnal tides in the southern SCS, where diurnal internal tides are more energetic during the summer and winter months, when monsoonal winds are incidentally stronger (Shang et al., 2015). The modulation of K_1 and P_1 thus enhances diurnal currents during the monsoon seasons when wind stress is also greater. This could help to elucidate the seasonal variation of the K_1 amplitude (Fig. 9) and its correlation with diurnal wind stress (Fig. 8). Moreover, the seasonality could also be augmented by potential resonant dynamics as the dominant frequency of diurnal wind stress and the K_1 frequency are largely similar, thereby establishing the role of wind stress in introducing nontidal energy at the K_1 frequency. This finding corroborates with prior results presented by Álvarez et al. (2003) and Dusek et al. (2017), both of whom concluded that changes in the sea breeze wind stress is responsible for the seasonal variations of the K_1 amplitude of estuarine tidal currents in Cádiz Bay, Spain, and Tampa Bay, Florida, respectively.

The phase relationship between currents and winds also exhibits nonstationary behaviour (Fig. 8). During the SW monsoon, the effect of diurnal wind forcing at Hantu East, Hantu South, and Kusu North is immediate as implied by the in-phase relationship. We speculate that as both the coastline and the major axis wind stress are oriented north-eastward, they are more aligned with each other, thereby facilitating current flow along that direction. However, Hantu North and Kusu East sites are oriented north-westward and hence the response to wind forcing is not immediate. Additionally, the anti-phase relationship observed in Hantu North implies negative correlation, which could be attributed to the currents flowing southward facing

resistance from the local winds blowing north and thus weakening in strength. Nevertheless, the orientation of the coastlines does not seem to be sufficient as the phase relationship over the entire year or so remains unclear. Compared to lower frequencies, there are huge fluctuations in the phase relationship at tidal frequencies (Fig. 8). Non-linear interactions between tides due to bottom friction, as well as between tidal and non-tidal forcing, can cause distortions in amplitude and phase lag of tidal constituents especially in shallow waters with a complex bathymetry (Wei et al., 2023). Form drag, which occurs when the flow passes over a bathymetric obstacle, was found to be more than twice the frictional drag and thus was the main cause for the sharp decline of tidal amplitudes over Reversing Falls (Horwitz et al., 2021). Hence, tidal currents are unusually weak at Kusu South, where there is steeper bathymetry (Fig. 1), as more energy was lost in overcoming the vertical pressure gradient.

The findings of spectral analysis underscore the importance of obtaining longer time-series, especially since regions at lower frequencies in the CWT and WC plots are strong and significant. However, we are constrained by the length of observational data and are thus only able to analyse signals with periods of up to 2 months, any period longer than that rendered unreliable due to edge effects that arise when performing wavelet analysis of low frequency signals. With longer datasets, we can better determine the effects of not only monsoons but other atmospheric forcing occurring at longer time scales such as the ENSO on currents. Such events are projected to intensify due to the increase in land–sea temperature contrast associated with climate change (Kitoh, 2017), with considerable changes in the strength of currents (Sen Gupta et al., 2021).

5 Conclusions

In this study, we investigated the nonstationary behaviour of coastal currents and their main drivers in Singapore. Despite the study sites being in close proximity, the variations in speed, PSD, CWT of alongshore currents, and WC between that and major axis winds revealed substantial heterogeneity across time and space. Current speeds in Hantu East and Hantu West consistently exceeded 100 cm s^{-1} during spring tides, while that in Hantu North, Hantu South and Kusu West only exceeded 100 cm s^{-1} in spring tides monthly during the monsoon seasons. Currents in the rest of the sites in Kusu Island are generally weak. Tides and winds are the two dominant mechanisms, the former accounting for 14–45 % of the total variance of currents for all study sites from the PSD plots. CWT not only displayed high power observed at tidal and low frequencies, but also elucidated the nonstationary behaviour as the strength of currents flowing at these frequencies exhibited temporal variation. At low frequencies of about 30–60 days, currents strengthen and propagate in phase with the winds during the NE monsoon when the MJO is more active. Meanwhile, the semi-annual variation of the K_1 amplitude and the correlation between diurnal currents and wind stress could be primarily attributed to the P_1 current, whose interaction with the K_1 current results in stronger diurnal currents despite its smaller amplitude. We also speculate that the seasonality of the K_1 amplitude is further reinforced by potential resonant dynamics with diurnal winds by virtue of having similar frequencies. However, the phase relationship between diurnal currents and winds fluctuates wildly and can only be partially explained by the orientation of the coastlines in relation to the wind direction, as currents in shallow waters are susceptible to being distorted by the local bathymetry.

445

The amplification of diurnal currents in response to the land–sea breeze has wider implications for nearshore sediment dynamics and coral reef ecosystems in the Singapore Strait. Stronger currents create higher shear stress at the seabed and are thus responsible for the increased resuspension of fine sediment (Fearon et al., 2020). In western islands such as Pulau Hantu where diurnal currents are stronger, coral reefs become more vulnerable to the effects of higher turbidity due to the decrease

450 in available habitat for growth (Morgan et al., 2020). Meanwhile, Kusu Island is reported to be one of the most robust sources of coral larvae seeding as it is situated upstream from the dominant current flowing net westward in the Singapore Strait (Tay et al., 2012). Given how coral reef larvae are heavily reliant on currents for dispersal (Tay et al., 2012), a deepened understanding of surface current variability will help reef management adopt targeted measures in conserving coastal areas with high seeding potential. Careful attention should also be given to the response of coral reef larvae to increased wind speeds,

455 particularly since the localised high correlation between currents and winds during the monsoon seasons can be observed from the WC analysis. The wavelet techniques employed here can not only provide insights to time dependent dynamics of coastal currents, but also in other oceanographic processes not limited to coral larvae transport as mentioned earlier, sediment dynamics, and internal tides. The consideration of nonstationary behaviour is therefore paramount in understanding the dynamics of coastal currents across different time scales.

460

Code and data availability

ERA5 hourly wind data at 0.25° x 0.25° resolution, not downscaled, are publicly available and can be downloaded from https://cds.climate.copernicus.eu/cdsapp#!/dataset/reanalysis-era5-single-levels?tab=overview. The database is available through an unrestricted data repository (DR-NTU) hosted by Nanyang Technological University

465 (https://doi.org/10.21979/N9/ICJXJ3) (Puah et al., 2024).

Author contributions

JYP performed all statistical analysis, developed the code, created the figures, and drafted the manuscript. IDS provided advice on paper structure. KM collected the observational data. DL, DP and MW provided general direction of the paper. ADS

470 provided direction for conceptualisation. All authors contributed to the scientific discussion of methods and results, as well as the editing of the manuscript.

Competing interests

The authors declare that they have no conflict of interest.

475

Acknowledgements

This Research/Project is supported by the National Research Foundation, Singapore, National Environment Agency, Singapore, under the National Sea Level Programme Funding Initiative (Award No. USS-IF-2020-2). This work comprises

EOS contribution number 569. We also like to thank Dr Srivatsan Vijayaraghavan from Tropical Marine Science Institute for
480 providing the downscaled wind data and the methods used in downscaling. The tide gauge data are provided from the Singapore
Maritime Port Authority. Colormaps are from the cmocean package (Thyng et al., 2016).

References

Álvarez, O., Tejedor, B., Tejedor, L., and Kagan, B. A.: A note on sea-breeze-induced seasonal variability in the K1 tidal
constants in Cádiz Bay, Spain, Estuarine, Coastal and Shelf Science, 58, 805–812, https://doi.org/10.1016/s0272-
485 7714(03)00186-0, 2003.

Amante, C. and Eakins, B. W.: ETOPO1 1 Arc-Minute Global Relief Model: Procedures, Data Sources and Analysis, NOAA
Technical Memorandum NESDIS NGDC-24, National Geophysical Data Center, NOAA [data set],
doi:10.7289/V5C8276M (last access: 1 June 2024), 2009.

Brunner, K. and Lwiza, K. M. M.: Tidal velocities on the Mid-Atlantic Bight continental shelf using high-frequency radar,
490 Journal of oceanography, 76, 289–306, https://doi.org/10.1007/s10872-020-00545-7, 2020.

Cervantes, O., Verduzco-Zapata, G., Botero, C., Olivos-Ortiz, A., Chávez-Comparan, J. C., and Galicia-Pérez, M.:
Determination of risk to users by the spatial and temporal variation of rip currents on the beach of Santiago Bay, Manzanillo,
Mexico: Beach hazards and safety strategy as tool for coastal zone management, Ocean & Coastal Management, 118, 205–
214, https://doi.org/10.1016/j.ocecoaman.2015.07.009, 2015.

495 Chen, H., Malanotte-Rizzoli, P., Koh, T.-Y., and Song, G.: The relative importance of the wind-driven and tidal circulations
in Malacca Strait, Continental Shelf Research, 88, 92–102, https://doi.org/10.1016/j.csr.2014.07.012, 2014.

Chen, M., Murali, K., Khoo, B.-C., Lou, J., and Kumar, K.: Circulation modelling in the Strait of Singapore, Journal of Coastal
research, 21, 960–972, https://doi.org/10.2112/04-0412.1, 2005.

Churchill, J. H., Lentz, S. J., Farrar, J. T., and Abualnaja, Y.: Properties of Red Sea coastal currents, Continental Shelf
500 Research, 78, 51–61, https://doi.org/10.1016/j.csr.2014.01.025, 2014.

Codiga, D. L.: Unified tidal analysis and prediction using the UTide Matlab functions,
https://doi.org/10.13140/RG.2.1.3761.2008, 2011.

Cosoli, S., Gačić, M., and Mazzoldi, A.: Surface current variability and wind influence in the northeastern Adriatic Sea as
observed from high-frequency (HF) radar measurements, Continental Shelf Research, 33, 1–13,
505 https://doi.org/10.1016/j.csr.2011.11.008, 2012.

Covey, C. and Barron, E.: The role of ocean heat transport in climatic change, Earth-Science Reviews, 24, 429–445,
https://doi.org/10.1016/0012-8252(88)90065-7, 1988.

Devlin, A. T., Jay, D. A., Talke, S. A., and Zaron, E.: Can tidal perturbations associated with sea level variations in the western
Pacific Ocean be used to understand future effects of tidal evolution?, Ocean Dynamics, 64, 1093–1120,
510 https://doi.org/10.1007/s10236-014-0741-6, 2014.

Devlin, A. T., Zaron, E. D., Jay, D. A., Talke, S. A., and Pan, J.: Seasonality of Tides in Southeast Asian Waters, Journal of
Physical Oceanography, 48, 1169–1190, https://doi.org/10.1175/JPO-D-17-0119.1, 2018.

Dusek, G., Park, J., and Paternostro, C.: Seasonal variability of tidal currents in Tampa Bay, Florida, Journal of Waterway, Port, Coastal, and Ocean Engineering, 143, 04016023, https://doi.org/10.1061/(ASCE)WW.1943-5460.0000373, 2017.

515 Fearon, G., Herbette, S., Veitch, J., Cambon, G., Lucas, A. J., Lemarié, F., and Vichi, M.: Enhanced Vertical Mixing in Coastal Upwelling Systems Driven by Diurnal-Inertial Resonance: Numerical Experiments, JGR Oceans, 125, e2020JC016208, https://doi.org/10.1029/2020JC016208, 2020.

Flinchem, E. P. and Jay, D. A.: An introduction to wavelet transform tidal analysis methods, Estuarine, Coastal and Shelf Science, 51, 177–200, https://doi.org/10.1006/ecss.2000.0586, 2000.

520 Foreman, M. G. G. and Henry, R. F.: The harmonic analysis of tidal model time series, Advances in water resources, 12, 109–120, https://doi.org/10.1016/0309-1708(89)90017-1, 1989.

GEBCO Compilation Group: GEBCO 2023 Grid [data set], https://doi.org/10.5285/f98b053b-0cbc-6c23-e053-6c86abc0af7b, 2023.

Grinsted, A., Moore, J. C., and Jevrejeva, S.: Application of the cross wavelet transform and wavelet coherence to geophysical 525 time series, Nonlinear processes in geophysics, 11, 561–566, https://doi.org/10.5194/npg-11-561-2004, 2004.

Grinsted, A.: Cross wavelet and wavelet coherence (https://github.com/grinsted/wavelet-coherence), Github, 2023. Retrieved December 6, 2023.

Guo, L., van der Wegen, M., Jay, D. A., Matte, P., Wang, Z. B., Roelvink, D., and He, Q.: River-tide dynamics: Exploration of nonstationary and nonlinear tidal behavior in the Yangtze River estuary, Journal of Geophysical Research: Oceans, 120, 530 3499–3521, https://doi.org/10.1002/2014JC010491, 2015.

Hasan, G. J., van Maren, D. S., and Cheong, H. F.: Improving hydrodynamic modeling of an estuary in a mixed tidal regime by grid refining and aligning, Ocean Dynamics, 62, 395–409, https://doi.org/10.1007/s10236-011-0506-4, 2012.

Hasan, G. J., van Maren, D. S., and Fatt, C. H.: Numerical study on mixing and stratification in the ebb-dominant Johor Estuary, Journal of coastal research, 29, 201–215, 2013.

535 Hasan, G. J., van Maren, D. S., and Ooi, S. K.: Hydrodynamic modeling of Singapore's coastal waters: Nesting and model accuracy, Ocean Modelling, 97, 141–151, https://doi.org/10.1016/j.ocemod.2015.09.002, 2016.

Hersbach, H., Bell, B., Berrisford, P., Hirahara, S., Horányi, A., Muñoz-Sabater, J., Nicolas, J., Peubey, C., Radu, R., and Schepers, D.: The ERA5 global reanalysis, Quarterly Journal of the Royal Meteorological Society, 146, 1999–2049, https://doi.org/10.1002/qj.3803, 2020.

540 Hijmans, R. and University of California, Berkeley, Museum of Vertebrate Zoology: Global Administrative Areas 2015 (v2.8) – Boundary, Malaysia, 2015, UC Berkeley, Museum of Vertebrate Zoology [data set], http://purl.stanford.edu/bd012vf3991, 2015.

Hoitink, A. J. F. and Jay, D. A.: Tidal river dynamics: Implications for deltas, Reviews of Geophysics, 54, 240–272, https://doi.org/10.1002/2015RG000507, 2016.

545 Horsburgh, K. J. and Wilson, C.: Tide-surge interaction and its role in the distribution of surge residuals in the North Sea, Journal of Geophysical Research: Oceans, 112, https://doi.org/10.1029/2006JC004033, 2007.

Horwitz, R. M., Taylor, S., Lu, Y., Paquin, J.-P., Schillinger, D., and Greenberg, D. A.: Rapid reduction of tidal amplitude due to form drag in a narrow channel, Continental Shelf Research, 213, 104299, https://doi.org/10.1016/j.csr.2020.104299, 2021.

550   Humanitarian Data Exchange: Indonesia - Subnational Administrative Boundaries, OCHA Services: Humanitarian Data Exchange [data set], https://data.humdata.org/dataset/cod-ab-idn, n.d.

Jay, D. A. and Flinchem, E. P.: Wavelet transform analyses of non-stationary tidal currents, in: Proceedings of The IEEE Fifth Working Conference on Current Measurement, 100–105, https://doi.org/10.1109/CCM.1995.516158, 1995.

Kang, S. K., Foreman, M. G. G., Lie, H.-J., Lee, J.-H., Cherniawsky, J., and Yum, K.-D.: Two-layer tidal modeling of the Yellow and East China Seas with application to seasonal variability of the M2 tide, Journal of Geophysical Research: Oceans,
555   107, 6-1-6–18, https://doi.org/10.1029/2001JC000838, 2002.

Kitoh, A.: The Asian monsoon and its future change in climate models: A review, Journal of the Meteorological Society of Japan. Ser. II, 95, 7–33, https://doi.org/10.2151/jmsj.2017-002, 2017.

Klemas, V.: Remote sensing techniques for studying coastal ecosystems: An overview, Journal of Coastal Research, 27, 2–17, 2011.

560   Large, W. G. and Pond, S.: Open ocean momentum flux measurements in moderate to strong winds, Journal of physical oceanography, 11, 324–336, https://doi.org/10.1175/1520-0485(1981)011<0324:OOMFMI>2.0.CO;2, 1981.

Li, X.-X., Koh, T.-Y., Panda, J., and Norford, L. K.: Impact of urbanization patterns on the local climate of a tropical city, Singapore: An ensemble study, Journal of Geophysical Research: Atmospheres, 121, 4386–4403, https://doi.org/10.1002/2015JD024452, 2016.

565   Lilly, J. M.: jLab: A data analysis package for Matlab, v. 1.6.6, http://www.jmlilly.net/jmlsoft.html, 2019.

Losada, M. A., Díez-Minguito, M., and Reyes-Merlo, M.: Tidal-fluvial interaction in the Guadalquivir River Estuary: Spatial and frequency-dependent response of currents and water levels, Journal of Geophysical Research: Oceans, 122, 847–865, https://doi.org/10.1002/2016JC011984, 2017.

Lowell, N. S., Walsh, D. R., and Pohlman, J. W.: A Comparison of tilt current meters and an acoustic doppler current meter
570   in Vineyard Sound, Massachusetts, in: 2015 IEEE/OES Eleventh Current, Waves and Turbulence Measurement (CWTM), 1–7, https://doi.org/10.1109/CWTM.2015.7098135, 2015.

Madden, R. A. and Julian, P. R.: Detection of a 40–50 Day Oscillation in the Zonal Wind in the Tropical Pacific, Journal of the Atmospheric Sciences, 28, 702–708, https://doi.org/10.1175/1520-0469(1971)028<0702:DOADOI>2.0.CO;2, 1971.

Martin, P., Moynihan, M. A., Chen, S., Woo, O. Y., Zhou, Y., Nichols, R. S., Chang, K. Y., Tan, A. S., Chen, Y.-H., and Ren,
575   H.: Monsoon-driven biogeochemical dynamics in an equatorial shelf sea: Time-series observations in the Singapore Strait, Estuarine, Coastal and Shelf Science, 270, 107855, https://doi.org/10.1016/j.ecss.2022.107855, 2022.

Morgan, K. M., Moynihan, M. A., Sanwlani, N., and Switzer, A. D.: Light limitation and depth-variable sedimentation drives vertical reef compression on turbid coral reefs, Frontiers in Marine Science, 7, 571256, https://doi.org/10.3389/fmars.2020.571256, 2020.

580   Müller, M.: The influence of changing stratification conditions on barotropic tidal transport and its implications for seasonal and secular changes of tides, Continental Shelf Research, 47, 107–118, https://doi.org/10.1016/j.csr.2012.07.003, 2012.

NASA JPL: NASA Shuttle Radar Topography Mission Global 1 arc second, NASA EOSDIS Land Processes Distributed Active Archive Center [data set], https://doi.org/10.5067/MEaSUREs/SRTM/SRTMGL1.003 (last access: 8 January 2024), 2013.

585 Navionics: Navionics ChartViewer, https://webapp.navionics.com, 2023.

Pawlowicz, R., Beardsley, B., and Lentz, S.: Classical tidal harmonic analysis including error estimates in MATLAB using T_TIDE, Computers & Geosciences, 28, 929–937, https://doi.org/10.1016/S0098-3004(02)00013-4, 2002.

Peng, D., Soon, K. Y., Khoo, V. H., Mulder, E., Wong, P. W., and Hill, E. M.: Tidal asymmetry and transition in the Singapore Strait revealed by GNSS interferometric reflectometry, Geoscience Letters, 10, 39, https://doi.org/10.1186/s40562-023-00294-590 7, 2023.

Percival, D. B. and Walden, A. T.: Spectral analysis for physical applications, cambridge university press, 1993.

Puah, J. Y., Haigh, I. D., Lallemant, D., Morgan, K., Peng, D., Watanabe, M., and Switzer, A. D.: Replication Data for: Importance of tides and winds in influencing the nonstationary behaviour of coastal currents in offshore Singapore (4), https://doi.org/10.21979/N9/ICJXJ3, 2024.

595 Pugh, D. T.: Tides, surges and mean sea level, 1987.

Robertson, A. W., Moron, V., Qian, J.-H., Chang, C.-P., Tangang, F., Aldrian, E., Koh, T. Y., and Liew, J.: The Maritime Continent Monsoon, in: World Scientific Series on Asia-Pacific Weather and Climate, vol. 5, WORLD SCIENTIFIC, 85–98, https://doi.org/10.1142/9789814343411_0006, 2011.

Sassi, M. G. and Hoitink, A. J. F.: River flow controls on tides and tide-mean water level profiles in a tidal freshwater river, 600 Journal of Geophysical Research: Oceans, 118, 4139–4151, https://doi.org/10.1002/jgrc.20297, 2013.

Sen Gupta, A., Stellema, A., Pontes, G. M., Taschetto, A. S., Vergés, A., and Rossi, V.: Future changes to the upper ocean Western Boundary Currents across two generations of climate models, Scientific reports, 11, 9538, https://doi.org/10.1038/s41598-021-88934-w, 2021.

Shang, X., Liu, Q., Xie, X., Chen, G., and Chen, R.: Characteristics and seasonal variability of internal tides in the southern 605 South China Sea, Deep Sea Research Part I: Oceanographic Research Papers, 98, 43–52, https://doi.org/10.1016/j.dsr.2014.12.005, 2015.

Singapore Land Authority: 2019 version of the 10-meter Digital Terrain Model (DTM) map of Singapore [data set], 2019.

Skamarock, W. C., Klemp, J. B., Dudhia, J., Gill, D. O., Liu, Z., Berner, J., Wang, W., Powers, J. G., Duda, M. G., and Barker, D. M.: A description of the advanced research WRF version 4, NCAR tech. note ncar/tn-556+ str, 145, 610 https://doi.org/doi:10.5065/1dfh-6p97, 2019.

Tay, Y. C., Todd, P. A., Rosshaug, P. S., and Chou, L. M.: Simulating the transport of broadcast coral larvae among the Southern Islands of Singapore, Aquatic Biology, 15, 283–297, https://doi.org/10.3354/ab00433, 2012.

Thomson, R. E. and Emery, W. J.: Data analysis methods in physical oceanography, Newnes, 2014.

Thyng, K., Greene, C., Hetland, R., Zimmerle, H., and DiMarco, S.: True Colors of Oceanography: Guidelines for Effective 615 and Accurate Colormap Selection, Oceanog, 29, 9–13, https://doi.org/10.5670/oceanog.2016.66, 2016.

Tkalich, P., Vethamony, P., Babu, M. T., and Malanotte-Rizzoli, P.: Storm surges in the Singapore Strait due to winds in the South China Sea, Natural hazards, 66, 1345–1362, https://doi.org/10.1007/s11069-012-0211-8, 2013.

Torrence, C. and Compo, G. P.: A practical guide to wavelet analysis, Bulletin of the American Meteorological society, 79, 61–78, https://doi.org/10.1175/1520-0477(1998)079<0061:APGTWA>2.0.CO;2, 1998.

620 Ursella, L., Poulain, P.-M., and Signell, R. P.: Surface drifter derived circulation in the northern and middle Adriatic Sea: Response to wind regime and season, Journal of Geophysical Research: Oceans, 111, https://doi.org/10.1029/2005JC003177, 2006.

Van Maren, D. S. and Gerritsen, H.: Residual flow and tidal asymmetry in the Singapore Strait, with implications for resuspension and residual transport of sediment, Journal of Geophysical Research: Oceans, 117, 625 https://doi.org/10.1029/2011JC007615, 2012.

Wang, D., Pan, H., Jin, G., and Lv, X.: Seasonal variation of the principal tidal constituents in the Bohai Sea, Ocean Science, 16, 1–14, https://doi.org/10.5194/os-16-1-2020, 2020.

Wei, Z., Jiao, X., Du, Y., Zhang, J., Pan, H., Wang, G., Wang, D., and Wang, Y. P.: The temporal variations in principal and shallow-water tidal constituents and their application in tidal level calculation: An example in Zhoushan Archipelagoes with 630 complex bathymetry, Ocean & Coastal Management, 237, 106516, https://doi.org/10.1016/j.ocecoaman.2023.106516, 2023.

Xue, Z., He, R., Liu, J. P., and Warner, J. C.: Modeling transport and deposition of the Mekong River sediment, Continental Shelf Research, 37, 66–78, https://doi.org/10.1016/j.csr.2012.02.010, 2012.

Zaytsev, O., Rabinovich, A. B., Thomson, R. E., and Silverberg, N.: Intense diurnal surface currents in the Bay of La Paz, Mexico, Continental Shelf Research, 30, 608–619, https://doi.org/10.1016/j.csr.2009.05.003, 2010.

635 Zhang, C.: Madden-Julian Oscillation, Reviews of Geophysics, 43, 2004RG000158, https://doi.org/10.1029/2004RG000158, 2005.Zhang, Q. Y.: Comparison of two three-dimensional hydrodynamic modeling systems for coastal tidal motion, Ocean Engineering, 33, 137–151, https://doi.org/10.1016/j.oceaneng.2005.04.008, 2006.

Zhu, Z.-N., Zhu, X.-H., Zhang, C., Chen, M., Wang, M., Dong, M., Liu, W., Zheng, H., and Kaneko, A.: Dynamics of tidal and residual currents based on coastal acoustic tomography assimilated data obtained in Jiaozhou Bay, China, Journal of 640 Geophysical Research: Oceans, 126, e2020JC017003, https://doi.org/10.1029/2020JC017003, 2021.